BIOCHEMISTRY
including biophysical chemistry & molecular biology

Article

Dissecting the binding between glutamine synthetase and its two natively unfolded protein inhibitors

David Pantoja-Uceda, Jose Luis Neira, Lorena Saelices, Rocío Robles-Rengel, Francisco J. Florencio, M. Isabel Muro-Pastor, and Jorge Santoro

Biochemistry, **Just Accepted Manuscript** • DOI: 10.1021/acs.biochem.6b00072 • Publication Date (Web): 27 May 2016

Dissecting the binding between glutamine synthetase and its two natively unfolded protein inhibitors[†]

David Pantoja-Uceda[‡,1,*], José L. Neira[#,$,1,*], Lorena Saelices[‖,¶], Rocío Robles-Rengel[‖], Francisco J. Florencio[‖], M. Isabel Muro-Pastor[‖] and Jorge Santoro[‡]

[‡] *Instituto de Química Física Rocasolano (IQFR), CSIC, Madrid;* [#]*Instituto de Biología Molecular y Celular, Universidad Miguel Hernández, Elche (Alicante)*; [$]*Instituto de Biocomputación y Física de Sistemas Complejos (BIFI), Unidad Asociada IQFR-CSIC-BIFI, Universidad de Zaragoza, Zaragoza;* [‖]*Instituto de Bioquímica Vegetal y Fotosíntesis, CSIC-Universidad de Sevilla, Seville, Spain.*

Short title: Binding of GS to IFs

[1]These two authors contributed equally to this work.

[¶]Current address: Department of Biological Chemistry, and Molecular Biology Institute, University of California, Los Angeles, Los Angeles CA 90095-1570, USA

*Corresponding authors' addresses: David Pantoja-Uceda, Instituto de Química Física Rocasolano, CSIC, 28006 Madrid, Spain. Tel: + 34 917459500. Email: dpantoja@iqfr.csic.es. José L. Neira, Instituto de Biología Molecular y Celular, Universidad Miguel Hernández, Avda. del Ferrocarril s/n, 03202 Elche (Alicante), Spain. Tel: + 34 966658459. E-mail: jlneira@umh.es.

Keywords: assignment; binding; biolayer interferometry; disorder; glutamine synthetase; NMR.

[†]Founding source: This work was supported by the Spanish Ministerio de Economia y Competitividad (CTQ2014-52633-P to DP-U; CTQ 2015-64445-R to JLN; and BFU2013-41712-P to MIM-P and FJF, with Fondo Social Europeo (ESF)), Junta de Andalucía (BIO-284 to FJF) and Generalitat Valenciana (Prometeo 018/2013 to JLN).

Abbreviations used: BLI, biolayer interferometry; CD, circular dichroism; DSS 4,4-dimethyl-4-silapentane-1-sulfonic acid; GOGAT, glutamate synthase; GS, glutamine synthetase; HSQC, heteronuclear single quantum correlation; IDP, intrinsically disordered protein; IF, inactivating factor; IF7, the *Synechocystis* sp PCC 6803 65-residue-long IF of GS; IF17, the *Synechocystis* sp PCC 6803 149-residue-long IF of GS; K_D, dissociation constant; k_{on}, association rate constant of the binding reactions of IFs to GS; k_{off}, dissociation rate constant of the binding reactions of IFs to GS; NMR, nuclear magnetic resonance; NtcA, nitrogen-responsive regulatory protein; SSP, secondary structure propensity; TFE, 2,2,2-trifluoroethanol; TROSY, transverse relaxation optimized spectroscopy; TSP, sodium trimethylsilyl [2,2,3,3-$^2H_4$] propionate.

ABSTRACT

Ammonium is incorporated into carbon skeletons by the sequential action of glutamine synthetase (GS) and glutamate synthase (GOGAT) in cyanobacteria. The activity of *Synechocystis* sp. PCC 6803 GS type I is controlled by protein-protein interactions with two intrinsically disordered inactivating factors (IFs): the 65-residue-long (IF7) and the 149-residue-long (IF17) ones. In this work, we studied both the IF7 and IF17 by Nuclear Magnetic Resonance (NMR), and we described their binding to GS, by using NMR and biolayer interferometry (BLI). We assigned the backbone nuclei of all residues of IF7. Analyses of chemical shifts and the ^{15}N-{^{1}H}-NOEs at two field strengths suggest that IF7 region Thr3-Arg13, and a few residues around Ser27 and Phe41 populated helical conformations (although the percentage is smaller around Phe41). The 2D ^{1}H-^{15}N HSQC and CON experiments suggest that IF17 populated several conformations. We followed the binding between GS and IF7 by NMR at physiological pH, and the residues interacting firstly with IF7 were Gln6 and Ser27, belonging to those regions that appeared ordered in the isolated protein. We also determined the k_{on}s and k_{off}s for the binding reactions to GS of both IF7 and IF17, where the GS protein was bound to a biosensor. The measurements of the kinetic constants for the binding reaction of IF7 to GS suggest that: (i) binding does not follow a kinetic two-state model ($GS + IF7 \underset{k_{off}}{\overset{k_{on}[IF7]}{\rightleftharpoons}} GS:IF7$); (ii) there is a strong electrostatic component in the determined k_{on}; and, (iii) the binding is not diffusion-limited.

Assimilation of ammonium is the process by which nitrogen is incorporated into carbon skeletons. This process takes place in the majority of microorganisms by the sequential action of glutamine synthetase (GS) and glutamate synthase (GOGAT). GS is capable of catalyzing the ATP-dependent amidation of glutamic acid to yield glutamine. Then, GOGAT is able to transfer the amide group from glutamine to 2-oxoglutarate yielding two molecules of glutamic acid. This protein network (the so-called GS-GOGAT cycle) is therefore the connecting step between carbon and nitrogen metabolism[1,2].

In cyanobacteria, GS type I is modulated at the transcriptional and posttranscriptional levels, according to the nitrogen and carbon supplies in the environment[3]. The classical feedback inhibition, adenylylation/deadenylylation of GS, observed in other bacteria[4], does not occur in cyanobacteria. However, there is a post-translational regulatory mechanism involving protein-protein interactions with a 65-residue-long (IF7) and a 149-residue-long (IF17) inactivating proteins[5-7]. Analyses of mutant strains devoid of IF7, IF17 or both proteins have shown that each of these contribute to GS inactivation *in vivo*. A maximal level of inactivation *in vitro* has been observed when both proteins are present, although the presence of either of the two, without additional modifications, is enough for GS inactivation[5]. In the presence of ammonium, IF7 and IF17 are expressed and GS is inactivated; on the other hand, removal of ammonium leads to degradation of IF7 and IF17[8]. The expression of both IFs is modulated by NtcA, the main factor responsible for nitrogen control in cyanobacteria[3,9,10].

We have shown that isolated IF7 and IF17 from *Synechocystis* sp PCC 6803 are both intrinsically disordered proteins (IDPs)[11,12], with no interaction between them[12]. In general, IDPs have crucial roles in processes such as cell-cycle control, cellular signalling and transcription[13]. IDPs do not fold into a well-defined globular three-dimensional structure, but rather they adopt an

ensemble of rapidly inter-converting conformations, which often, but not always, acquire an ordered structure upon binding to their targets. Among the advantages conferred by disorder are specificity, without excessive binding strength and binding promiscuity[13,14]. Moreover, it is frequently stated that the most important advantage of intrinsic disorder is the potential for higher association rates (the so-called k_{on}s) of the IDP with its different partners[14]. However, recent reports have suggested that there is no experimental evidence to support that IDPs fold faster than their folded counterparts[15-18]. In fact, the reported k_{on}s span many orders of magnitude for both disordered and folded proteins, with no statistically difference between both groups of biomolecules[17], and thus, it seems that the k_{on}s reveal distinct, particular features of the IDPs involved in a binding reaction[18].

In this work, we describe the conformational preferences of IF7 at atomic level by using NMR techniques. The assignment of its backbone nuclei and the measurement of the ^{15}N-{^{1}H}-NOEs allowed us to determine which regions of the protein have an intrinsic tendency to become folded. The first half of the protein seems to populate helical conformations between residues Thr3-Arg13, but there is also evidence of folded conformations around residues Met25-Ala29 and Phe41-Thr43. Furthermore, the assignment allowed us to follow which residues interacted firstly with GS: Gln6 and Ser27, involved to those regions that appeared partially ordered. The NMR experiments with IF17 suggested that the protein had segments with different mobility and several conformations in solution. We also determined the k_{on}s and k_{off}s for the binding reactions to GS of both IF7 and IF17 by biolayer interferometry (BLI), where the GS protein was bound to a biosensor. The use of low urea concentrations in IF17 hampered any reliable conclusion on the kinetics mechanism of its binding reaction to GS. Our kinetic results with IF7 suggest that: (i) the binding of IF7 to GS is more complicated than the simplest kinetics two-state model; (ii) the apparent k_{on} has an important electrostatic component as shown by experiments in the presence of high concentrations of NaCl; and, (iii) the binding is not diffusion-limited, that is, the k_{on} is smaller than the usual value of 10^5-10^6 M^{-1} s^{-1} of the diffusion-controlled macromolecular interactions[19].

EXPERIMENTAL PROCEDURES

Materials: Deuterium oxide, deuterated TFE and non-deuterated TFE were obtained from Apollo Scientific (Stockport, UK). The sodium trimethylsilyl [2,2,3,3-$^{2}H_4$] propionate, TSP (used for indirect calibration in the 500 MHz magnet), and 4,4-dimethyl-4-silapentane-1-sulfonic acid, DSS (used in the 800 MHz magnet), were from Sigma (St. Louis, MO). Ultrapure urea was from MP Biomedicals (USA). Thrombin was purchased from GE (Healthcare, Spain). Dialysis tubing, with a molecular weight cut-off of 3500 Da, was from Spectrapor (Spectrum Laboratories, Japan). Amicon centrifugal devices with a molecular weight cut-off of 3500 Da were from Millipore (Millipore, MA). Standard suppliers were used for all other chemicals. Water was deionized and purified on a Millipore system.

Protein expression and purification: The recombinant GS, IF17 and IF7 proteins were expressed and purified as described by using His-tagged vectors[5,7,11,12]. Protein stocks were run in SDS-PAGE gels and found to be > 97% pure. The purified stock of IF17 contained 0.3 M urea, since otherwise IF17 was not soluble. Protein concentrations were determined from the absorbance of individual amino acids[20].

For the experiments in BLI, the His-tags of IF7 and IF17 were removed by using thrombin in the proper buffer (20 mM Tris, pH 8.4, 150 mM NaCl and 2.5 mM $CaCl_2$, which was supplemented with 0.3 M urea in the case of IF17). An amount of 3.5 units of thrombin per mg of protein was added for each protein and the resulting solution was incubated overnight at room temperature. Thrombin was separated from the cleavage reaction by using a Hi-trap benzamidine (GE Healthcare Spain) coupled to an AKTA-FPLC (GE Healthcare), following the absorbance at 280 nm.

NMR spectroscopy: The NMR data were either acquired on a Bruker Avance DRX-500 (Bruker GmbH, Germany) spectrometer equipped with a triple-resonance probe and z-gradients, and

on a Bruker AV 800 (Bruker GmbH, Germany) spectrometer equipped with an inverse triple-resonance TCI cryoprobe and z-gradients.

For the sequence-specific assignment of IF7, 1.7 mM of a uniformly ^{13}C- and ^{15}N-labelled sample in 10 mM acetic/acetate buffer, pH 4.5, and 9:1 H_2O:D_2O was used in the Bruker AV 800 at 25 ºC. The assignment was obtained by the combination of standard triple resonance techniques[21] using 2D ^{1}H-^{15}N HSQC and 3D HNCO, HN(CA)CO, intra-HNCA, HN(CO)CA, intra-HNCACB, CBCA(CO)NH and HBHA(CO)NH spectra, and ^{13}C detected methods using 2D CON, 3D (H)N(COCA)NCO and (HN)CO(CA)NCO spectra[22]. In addition, 2D experiments that provide amino acid type identification of the NH correlation signals of the ^{1}H-^{15}N HSQC spectrum were used to facilitate the assignment process[23,24]. The triple resonance experiments were acquired with 1 K complex points in the ^{1}H dimension, 24 complex points in the ^{15}N dimension and 45 or 50 complex points in the ^{13}C dimension, and 4 or 8 scans. The 3D ^{13}C detected spectra were acquired with 512 complex points in the ^{13}CO dimension and 28 complex points in either the ^{15}N or ^{13}CO dimensions, with 4 scans in all cases. The resulting matrix was zero-filled to double the number of original points in all dimensions and shifted squared sine-bell apodization functions were applied in all dimensions prior to Fourier transformation. The programs NMRPipe[25] and NMRView[26] were used for spectral processing and data analysis, respectively. ^{1}H chemical shifts were directly referenced to DSS. To avoid any interaction with our protein we used a 3 mm NMR tube filled with our protein sample; we put this tube inside a 5 mm NMR tube filled with DSS. The ^{13}C and ^{15}N chemical shifts were referenced as described[27]. The BMRB (Biological Magnetic Resonance Bank) accession number for the assignment of IF7 is 25921.

The ^{15}N-{^{1}H} NOEs of IF7 were measured at both magnetic fields at 25 ºC at the same protein concentration by recording interleaved spectra with and without proton saturation; proton saturation was achieved by a series of 120º pulses, separated by 5 ms delays. The spectra recorded in the presence of proton saturation were acquired with a saturation time of 10 s. The spectra recorded

without proton saturation incorporated a relaxation delay of 10 s. At 500 MHz, the number of complex data points in the ^{1}H dimension was 1 K and those in the ^{15}N one was 100; the number of scans was 128. The experimental set was the same as that in the ^{1}H-^{15}N HSQC experiments (see below). At 800 MHz, the number of complex data points in the ^{1}H dimension was 1 K and 64 complex points in the ^{15}N one, with 4 scans. The carrier in the ^{1}H dimension was set at the water frequency and that of the ^{15}N at 119.636 ppm. The spectral widths used were 12 and 18 ppm in the ^{1}H and ^{15}N dimensions respectively. The NOE ratio was defined as: NOE = I_{sat}/I_{ref}, where I_{sat} is the intensity of the corresponding cross-peak in the saturated spectrum and I_{ref} is that in the reference (non saturated) spectrum. Peak intensities in the 500 MHz were measured with XWIN-NMR software (Bruker) working on a PC computer and using NMRView[26] program in the spectra acquired in the 800 MHz. We calculated at each magnetic field the average and the standard deviation of all NOEs by removing those of the last two residues at the C terminus; those averages and standard deviations were used as cut-off to elucidate the more rigid residues at each field. Errors in the NOEs were estimated to be 10% as judged from the integrated regions where no peaks were observed.

Experiments to determine the residues of IF7 titrating upon addition of GS were also carried out in the Bruker AV 800 at 20 ºC, in the presence of 50 mM Tris, pH 7.0. Resonance assignment was extrapolated from pH 4.5. We decided to use pH 7.0 because at acidic pHs GS precipitated[11], and the temperature was decreased (see Results). It could be thought that we could choose a somewhat lower pH, but the CD and fluorescence results suggest that GS acquired a native-like conformation only at pH close to physiological (see Discussion). IF7 concentration in the titration experiments was 130 μM, and the final GS concentrations were 2.6, 5.2 and 80 μM. Each concentration of GS was prepared as a fresh new sample with the same amount (130 μM) of IF7. The titrations were followed by ^{1}H-^{15}N TROSY experiments. The spectra were acquired with 1 K complex points in the ^{1}H dimension, 64 complex points in the ^{15}N dimension, and 16 scans. The

carrier of the ^{1}H dimension was set at the water frequency, and that of ^{15}N at 117 ppm. The spectral widths used were 12 and 18 ppm in the ^{1}H and ^{15}N dimensions, respectively.

The ^{1}H-^{15}N HSQC spectrum at pH 4.5 in the presence of 60% TFE was acquired at 25 ºC with 1.6 mM of IF7 in the Bruker Avance DRX-500. This spectrum was acquired with spectral widths of 30 ppm in the ^{15}N dimension, and 12 ppm in the ^{1}H one; carrier frequency was set to 120 ppm (for ^{15}N) and 4.7 ppm (the water frequency for ^{1}H). The number of complex data points in the ^{1}H dimension was 1 K and those in the ^{15}N one was 100; the number of scans was 32.

Biolayer interferometry (BLI): The association (k_{on}) and dissociation (k_{off}) rate constants of the binding reactions of IF7 and IF17 to GS were determined by BioLayer Interferometry using a BLItz system (ForteBio, Pall, Spain)[28]. The GS (at 1.3 μM) was immobilized on His-tag biosensors (Forte Bio) previously hydrated with 10 x kinetics sample buffer (ForteBio, the 10 X kinetics sample buffer as supplied by the manufacturer was: PBS 1 x, pH 7.4, 10 mM phosphate; 150 mM NaCl; Tween 20 (0.02%); albumin (0.1%); and sodium azide (0.05%)). Experiments at low NaCl concentration were carried out in this buffer. In these, increasing amounts of protein (typically, 0.1; 1; 3; 5 and 10 μM) were used in the association steps. For the experiments in the presence of 5% TFE, we used the same range of protein concentrations for both IF7 and GS, in the same buffer, but adding a volume of pure TFE to yield a 5% final concentration. Usually, five to six sensors were used to record the kinetic titration series. For the experiments in the presence of NaCl, the final concentration was 0.450 M. The experiments with IF17 were carried out at similar protein concentrations as described above for IF7 and in the presence of 0.3 M urea to avoid protein precipitation. The response was monitored every 0.2 s in all cases. The sensorgrams were always referenced against the sole buffer reference signal, which was monitored at the beginning of each experiment.

The general scheme of the GS-association/dissociation reactions for both proteins was: 30 s of initial baseline with the 10 x kinetics buffer; 120 seconds of loading GS into the biosensor; 30 s of baseline with the 10 x kinetics buffer; 120 seconds of association of either IF7 or IF17 to the

biosensor (which had been previously loaded with GS); and 120 seconds of dissociation from the biosensor of either IF7 or IF17. Similar results to those described (see Results section) were obtained with 300 s of the association step. Base line reference, the initial curve fitting of the sensorgrams and preliminary K_D calculations were carried out with the BLItz Pro 1.2 software. It is important to indicate that in interferometry either at the beginning of the association or dissociation step there could be a "jump" (discontinuity) between the response units in the sensorgrams. These changes are due to the refractive index of the biosensor[29]. Such discontinuity is taken into account by the software of the manufacturer during fitting. Fitting of the curves was also carried out manually by using Kaleidagraph.

Fitting of the sensorgrams: The software of the manufacturer allows fitting the sensorgrams with a global or local analysis to the simplest kinetic 1:1 model, which for the binding reaction described in this work is:

$$\underset{(free)}{GS} + IF7 \underset{k_{off}}{\overset{k_{on}[IF7]}{\rightleftharpoons}} \underset{(complex)}{GS:IF7},$$

where k_{on} (M^{-1} s^{-1}) and k_{off} (s^{-1}) are the association and dissociation rate constants, respectively, and [IF7] is the concentration of the protein in the solution. The interferometry response during the association step, $R(t)$ (measured in resonance units, RU), and the binding rate, dR/dt, can be used to evaluate the kinetics of the GS-IF7 interaction, as[30-33]: $\frac{dR}{dt} = k_{on} \times [IF7] \times \left(R_{\max} - R(t)\right) - k_{off} \times R(t)$, where R_{max} is proportional to the total concentration of GS bound to the biosensor, and the interferometry response, $R(t)$, is given by: $R(t) = R_{eq} - R_{eq} \times \exp(-k_{obs} \times (t - 180))$, where R_{eq} is the steady-state, or equilibrium, response obtained at infinite time when dR/dt = 0. Therefore, the association step between IF7 and GS-biosensor-bound is fitted to a single exponential. The number 180 in the *R(t)* equation corresponds to the time at which the association step between GS-biosensor-bound and the IF7 in the solution starts, in our experimental design (see above). As we are under a pseudo-first-order regime, then the value of k_{obs} is: by: $k_{obs} = k_{on} \times [IF7] + k_{off}$. For the dissociation of

the bound IF7 in buffer, where [IF7] = 0, the $R(t)$ is: $R(t) = R_1 \times \exp(-k_{off} \times (t - 300))$, where the number 300 comes from the time in our experimental design where dissociation of IF7 from the biosensor starts (see above), and R_1 is the response level when dissociation starts at 300 s. Therefore, the dissociation step should be fitted to a single exponential with the expression given above. It must be noted that k_{off} can be obtained directly from the dissociation step, but k_{on} must be only obtained from the slope of the straight line of the k_{obs} under the pseudo-first-order conditions; in addition, the y-axis intercept of such straight line (pseudo-first-order plot) must equal the k_{off}.

In all cases assayed (in aqueous solution or in the presence of 5% TFE), there were not large differences between both local and global fittings (less than 10%) provided by the software, and then, the global fittings were used in all cases. The global χ^2 was, however, not good enough and then, we decided to carry out the fittings of each [IF7] by using Kaleidagraph working on a PC. In most IFs concentrations, we used two exponential curves for data fitting in the association step (either in aqueous solution (at the two NaCl concentrations) or in the presence of 5% TFE): $R(t) = R_{eq} - R_{eq} \times \exp(-k_{obs} \times (t - 180)) - R'_{eq} \times \exp(-k'_{obs} \times (t - 180))$; with this equation we are assuming that the equilibrium response at infinite time (that is, R_{eq}) is attained with the fastest k_{obs}. For the higher IF7 concentrations used, 3, 5 and 10 μM (see Results), we observed a downward slope as the time increased, after reaching the equilibrium, either in the presence or in the absence of TFE. According to the manufacturer, this is due to the formation of a second layer of IF7 protein on the surface of the biosensor, which as it is not bound to GS, it slowly comes off from the biosensor. In these three IF7 concentrations, we fitted the association data to an exponential with a slope (K) baseline: $R(t) = R_{eq} - R_{eq} \times \exp(-k_{obs} \times (t - 180)) - K(t - 180)$. This situation in BLI is similar to that found in other techniques used to detect binding, such as stopped-flow, where at the long observation times photo-bleaching is observed and fitted as a straight line with negative slope. Manual fitting using Kaleidagraph had, in all analyzed curves, regression coefficients larger than

0.999 and the residuals did not show any tendency for any fitting. The reported uncertainty in the rate constants are fitting errors.

Circular dichroism (CD): Far-UV CD measurements of IF7 at different TFE concentrations (from 0 to 60% (vol/vol)) were carried out on a Jasco J-815 spectro-polarimeter (Jasco, Japan) controlled with a Peltier at 25 ºC. The experimental set was as described[11]. IF7 concentration was 20 μM in 10 mM acetate buffer (pH 4.5). Blank corrections were made in all spectra. The TFE titration was repeated twice with a fresh new sample.

In the pH-denaturation experiments of GS, the experimental set was the same as that used for the TFE titrations of IF7. Protein concentration was 0.9 μM (in protomer units). The pH of each sample was measured after completion of the experiments with an ultra-thin Aldrich electrode in a Radiometer (Copenhagen) pH-meter. The salts and acids used were: pH 2.0-3.0, phosphoric acid; pH 3.0-4.0, formic acid; pH 4.0-5.5, acetic acid; pH 6.0-7.0, NaH_2PO_4; pH 7.5-9.0, Tris acid; pH 9.5-11.0, Na_2CO_3; pH 11.5-13.0, Na_3PO_4. The titration was repeated twice.

For the thermal denaturation experiments in 60% TFE, ellipticity at 222 nm was recorded as temperature was increased at a scan rate of 1 °C/min from 25 to 85 °C. Acquisition parameters were: 1 nm of bandwidth, 8 s of response time and a 0.2 °C data pitch. Experiments were carried with 20 μM of protein. The thermal denaturation was repeated twice with a fresh new sample.

Fluorescence: Measurements of IF7 at different TFE concentrations (from 0 to 80% (vol/vol)) were carried out at 25 ºC on a Cary Varian spectrofluorimeter (Agilent, USA), interfaced with a Peltier temperature controller. Protein concentrations were 5 μM. Protein samples were excited at 280 and 295 nm in 10 mM acetate buffer (pH 4.5). The experimental set was as described[11,12] . Blank corrections were made in all spectra. The TFE titration was repeated twice with a fresh new sample.

In the pH-denaturation experiments of GS, the experimental set was the same as that used for the TFE titrations of IF7. Protein concentration was 1 μM (in protomer units). The pH of each sample was measured after completion of the experiments with an ultra-thin Aldrich electrode in a

Radiometer (Copenhagen) pH-meter. The salts and acids used were the same as in the CD experiments. The titration was repeated twice.

Control experiments of GS in the presence of 5% and 10% (v/v) TFE were acquired with the same experimental set described above. These experiments were carried out to ensure structural integrity of GS in the presence of the co-solvent. At 10% TFE, the fluorescence intensity of GS spectrum started decreasing (data not shown) and then, we carried out the BLI measurements to determine the binding of IF7 to GS at 5% TFE.

RESULTS

IF7 and its conformational features

We carried out the backbone assignment of IF7 by using NMR techniques developed for IDPs, since the ^{1}H-^{15}N HSQC spectrum showed signals with narrow lines and limited dispersion (Fig. 1). The use of those assignments in δ2D software[34] (www-mvsoftware.ch.cam.ac.uk) yields a prediction of helical populations (larger than 10%) between residues Gln4 to Arg13, Met25 to Ala29 and Phe41 to Thr43, whereas the rest of the protein seems to populate random-coil conformations (Fig. 2 middle). In total, the δ2D prediction suggests that 29% of the residues in IF7 adopt helical conformations (helical percentages larger than 10%) and a 71% of them populate random-coil conformations. Use of s2D, whose predictions rely only on the protein sequence[35], indicates that IF7 has a higher percentage of residues (88%) populating helical conformations (percentages of helix larger than 10%) (Fig. 2 bottom). However, in both predictions, the polypeptide regions with the highest percentages of helical conformation correspond to residues around Ala9 and Ser27.

The ^{15}N-{^{1}H} NOEs measured in IF7 showed very low values at 500 MHz and most of them were negative, suggesting that the protein was not ordered (Fig. 2 top, black line). Only regions Ala9-His14, around residue Leu26, and around Asp40 had values above 0.06 (the average was -0.03 ± 0.09); these polypeptide regions are within those predicted by δ2D and s2D to acquire some ordered structure. Measurements at 800 MHz (Fig. 2 top, grey line) were positive and showed also two regions with the highest values (above 0.44, the average was 0.34 ± 0.10) around Ala9 and Asp40. Comparison between the results at both fields suggests that the NOE profile was flatter at 800 MHz, as it has been observed in other IDPs[36].

Thus, taken together the analysis of chemical shifts, the analysis of the primary sequence and the NOE data, we suggest that the polypeptide regions of IF7 around Leu10 and Phe41 have an intrinsic tendency to populate helix-like conformations.

Since there is an intrinsic tendency to acquire helical conformations at the N terminus of IF7, we reasoned that the use of TFE could help to stabilize such populations. The 2,2,2-trifluoroethanol (TFE) is known for stabilizing pre-formed or marginally stable α-helices by mimicking the hydrophobic environment experienced by proteins in protein-protein interactions or within the tertiary structure of a protein[38]. To that end, we carried out TFE titrations by using fluorescence and far-UV CD. The fluorescence spectrum of isolated IF7 in aqueous solution has a maximum wavelength at ~350 nm[11]. As the concentration of TFE increased, there was a shift in the maximum of the spectrum towards blue-wavelengths (Supplementary Material Fig. 1 A, main panel). However, there was not a sigmoidal tendency in the fluorescence intensity at any of the explored wavelengths (Supplementary Material Fig. 1 A, inset). The far-UV CD of isolated IF7 has also been described before: it resembles that of an unfolded polypeptide chain, with a shoulder at 222 nm[11]. As the concentration of TFE was raised the absolute value of the raw ellipticity increased suggesting the acquisition of helical-like structure (Supplementary Material Fig. 1 B, main panel). In contrast to that observed by fluorescence intensity, the ellipticity at 222 nm followed a sigmoidal behaviour (Supplementary Material Figure 1 B, inset), with absence of native baseline at low concentrations of TFE. The fact that fluorescence and CD techniques did not show a similar titration behaviour suggests that the acquisition of helical structure is not a two-state process[38]. The highest ellipticity and, therefore, the highest population of helical structure, was observed at 60% TFE, but since the process is not two-state, the estimation of helical structure from the ellipticity at this co-solvent concentration would be unreliable. These results prompted us to acquire: (i) a far-UV CD thermal denaturation at 60% TFE to show the melting of the helical structure; and, (ii) a ^{1}H-^{15}N HSQC spectrum at 60% TFE to elucidate whether there was a spreading of amide cross-peaks under these conditions. The absence of sigmoidal behaviour in the thermal denaturation indicates that the helix-like structure suggested by far UV CD spectra, under these conditions, is not rigid (Supplementary Material Fig. 2 A), probably involving an un-cooperative melting of the different (partially-folded)

species populated. Moreover, the ^{1}H-^{15}N HSQC spectrum did not show a spreading of the resonances (Supplementary Material Fig. 2 B), and was similar to the spectrum of an isolated IDP protein in aqueous solution. These results suggest that the structure acquired at 60% TFE was not stable, and involves probably several conformations.

We also tried to assign IF17 in the presence of 0.3 M urea, but the ^{1}H-^{15}N HSQC and the CON spectra showed a smaller number of signals than could be expected (Supplementary Material Fig. 3). Furthermore, the intensity among the signals changed drastically suggesting that the protein had a sort of conformational-exchange equilibrium comprising several polypeptide patches. These unfavourable features hampered the assignment. As IF7 has a high sequence similarity with the C-terminal region of IF17[12] (Supplementary Material Fig. 4) (40.3% identity according to Blast[39] and Clustal[40]), in the absence of an assignment of IF17, we hypothesize that its C-terminal region also has a higher helical propensity than the rest of its polypeptide chain.

Residues of IF7 involved in binding to GS

Before following the titration of IF7 with GS by NMR, we carried out a temperature study at pH 7.0 (where the titration must be carried out, see below) of the signals of isolated IF7 to be sure which temperature should be used. Initially, we acquired 1D ^{1}H NMR spectra to monitor a wide range of temperatures from 5 to 35 ºC on the AV Bruker 800 MHz spectrometer. We used a ^{15}N-labeled sample, and thus we ran a decoupled version of 1D ^{1}H NMR experiment using 2048 data points for acquisition and 32 scans. We observed that when the temperature was increased (Supplemental Material Fig. 5 A), most of the signals became substantially broader and for some residues they disappeared in the amide region; however, the signals were not modified in the aliphatic region. These changes in the amide region are probably due to solvent-exchange, or alternatively, to variations in the population of different conformers in the IF7 upon increasing the temperature[41], or changes in the viscosity of the solution (and then, in the correlation time of the protein). Furthermore, we acquired (i) 2D ^{1}H-^{15}N HSQC spectra with water-flip-back to avoid water

saturation and then to minimize signal losses for labile protons; and, (ii) TROSY versions of the same experiments. The spectrum at pH 4.5 (Supplementary Material Fig. 5 B) contained a larger number of signals than at pH 7.0 (due to solvent-exchange). In addition, at pH 7.0, a larger number of signals was observed at the lower temperature (20 ºC), and clearly, the TROSY spectra contained more IF7 signals than the HSQC experiments. Therefore, as a compromise, we decided to carry out the GS-IF7 titration followed by NMR at 20 ºC, and by using a TROSY pulse sequence.

We carry out pH-denaturations of GS followed by intrinsic fluorescence and CD, to find out in which range of pH the protein acquired a native-like structure, since GS precipitates at low pH[11]. Our results show that GS acquired a minimum of ellipticity at 222 nm at physiological pH (Supplementary Material Fig. 6, blank, blue circles); in addition, the maximum of fluorescence intensity was acquired also at physiological pHs (Supplementary Material Fig. 6 blank, black circles). To conclude, both spectroscopic techniques indicate that GS only acquires native-like secondary and tertiary structures at physiological pHs, and then, we had to carry out our titration NMR experiments at pH 7.0 and 20 ºC (see above).

At this pH, the number of NMR observable signals of IF7 decreased dramatically (when compared to that at pH 4.5), because most of the amide protons are not hydrogen-bonded and they are not protected from solvent-exchange (Supplementary Material Fig. 5 A, first and second ^{1}H-^{15}N-HSQC spectra from the left in the figure). The amide protons observed at this pH (apart from the side-chains of Asn and Gln) were Gln4, Gln5, Gln6, Ala7, Arg8, Ala9, Leu10, Met11, Met12, Arg13, Gln16, Ile18, Ser27, Ala29, Ala30, Ala31, Glu32, Ile33, Gly34, Val35, Glu36, Ala37, Glu38, Lys39, Asp40, Phe41, Trp42, Thr43, Thr44, Val45, Gln46, Lys48, Phe53, Tyr57, Asp58, Arg59, Ser63 and Ser65. Many of these amino acids are close to, or are, an acidic residue, and thus, they could be hydrogen-bonded with the side-chain, and therefore protected from exchange with the solvent; the others have a bulky side chain, which could also hamper solvent-accessibility. In fact, it has been known for a long time that hydrogen-bonding and burial from solvent are the main reasons

behind solvent-protection[42]. It is interesting to note that most of the residues observed at pH 7.0 were those with the largest NOEs (see above), or predicted to populate helix-like conformations (Fig. 2), where the amide protons can be hydrogen-bonded (and thus solvent-protected) part of the time.

The binding of GS to IF7 was characterized using NMR chemical shift perturbations in 2D ^{1}H-^{15}N TROSY spectra of the above remaining signals. At this stage, it is interesting to note that holo and apo GS molecules are invisible to solution-state NMR due to its large size (GS is formed by 12 subunits of approximately 50 kDa organized in two hexameric rings[43]). Thus, the residues of IF7 important for binding to GS can be observed only when the exchange between the fully-bound IF7 and the free-state IF7 is sufficiently fast; otherwise, the cross-peaks will disappear upon binding to GS. Moreover, the magnitude of the changes in the cross-peaks of IF7 upon binding to GS will depend on: (i) the conformation and chemical environments for each particular residue; and (ii) the concentration of the bound species. Upon addition of 2.6 μM GS to the solution, the ^{1}H-^{15}N TROSY spectrum showed the disappearance of signals of Gln6 and Ser27 (Fig. 3 A). The ^{1}H-^{15}N TROSY at 5.2 μM of GS showed, in addition, the disappearance of Gln4, Gln5, Ala7, Arg8, Met12, Gln16, Gln46, Phe53, Arg59 and Ser63. The non-uniform broadening (and then, the disappearance of peaks) is caused by an exchange of IF7 molecules between their free and their GS-bound state that is intermediate within the NMR time scale (Fig. 3 B). The spectrum at the highest concentration of GS (80 μM) showed only the cross-peak of Ser65 (apart from the side chains of Asn and Gln). It could be thought that only the weakest signals in the spectrum of isolated IF7 disappeared first upon GS addition (Gln6 and Ser27), however, careful observation of Fig. 3B shows that it is not the case in the complex IF7:GS. For instance, Gln16, which also had the same absolute intensity as Gln6 in the spectrum of isolated IF7, remained at 2.6 μM of GS (Fig. 3 B). Moreover, residues Thr44 and Asp58 appear at the two GS concentrations shown (and they disappear at 80 μM of GS), whereas Ala7, Arg8, Met12 and Phe53, whose cross-peaks have an absolute intensity comparable to those of Thr44 and Asp58 in isolated IF7 (Fig. 3 B), do disappear in the presence of 5.2 μM of GS. Therefore,

although we cannot unambiguously rule out that there might be a slow exchange equilibrium, within the NMR timescale, from our data (the above commented differences in intensities among residues and how they differently disappear upon GS addition), we favor an intermediate exchange during the formation of the IF7:GS complex.

Thus, the residues interacting firstly with GS are those: (i) with the possibility to form hydrogen-bonds with their side-chain (a Gln and a Ser); and, (ii) belonging to the regions which seem to acquire helical structure in the isolated protein. At the different GS concentrations explored, our findings are also in agreement with previous fluorescence results from our groups, since the affinity constant of IF7 for GS could be determined by changes in fluorescence of the sole tryptophan (Trp42)[11]; accordingly, the NMR results in this work indicate that residues affected by the presence of GS are Phe41, Trp42 and Tyr57.

The kinetic parameters of the binding reaction of IF7 to GS

(a) *Experiments in aqueous solution at low ionic strength (150 mM)*: Since IF7 is an IDP, we were also interested in elucidating which are the rate constants of the binding reaction to GS to compare with the values reported in the literature for other IDPs[17]. From the software of the instrument, the k_{on} was (3.2 ± 0.2) x 10^4 M^{-1} s^{-1} and the k_{off} was (3.03 ± 0.07) x 10^{-2} s^{-1} both in 150 mM NaCl (the amount contained in the kinetic buffer) (Fig. 4 A). However, the fittings were not good enough, as judged from the global χ^2. Then, we fitted the association and dissociation steps for each IF7 concentration manually. Each association step for IF7 concentrations ranging from 0.16 μM to 1 μM could be fitted to two exponentials (Supplementary Material Fig. 7 A) suggesting that the binding to GS did not follow a simple 1:1 mechanism; at any IF7 concentration, the smallest k_{obs} of the two exponentials had always amplitudes that were between 10-20% of the amplitude of the fastest (i.e., the R_{eq}). For the larger concentrations of IF7 (i.e., 3, 5 and 10 μM) the fitted k_{obs} agreed with those of the larger amplitudes for the lower concentrations. Furthermore, at the smallest IF7

concentration (0.16 μM), the association curve of the sensorgram had not reached a plateau (equilibrium) (Supplementary Material Fig. 7 A), and then, it could be argued that the value of k_{obs} from the fitting to the two exponentials was not reliable enough. However, because of the large amount of acquired points (every 0.2 s), the fitting of the data converges to reliable values of k_{obs} and $R_{eq,}$ as it has been previously noted[33]; in fact, removal of the k_{obs} at this concentration in the pseudo-first-order plot does not modify the obtained values of the k_{on} and k_{off} (Supplementary Material Fig. 7 B).

The pseudo-first-order plot of the fastest k_{obs} (the exponential with the larger amplitude) yields a k_{on} of (4.7 ± 0.2) x 10^4 M^{-1} s^{-1} and a k_{off} of 1.9 ± 0.8 x 10^{-2} s^{-1} (Supplementary Material Fig. 7 B) (Table 1). The rate of both constants yields a K_D of 0.4 ± 0.2 μM, which is the same than that obtained by equilibrium fluorescence titrations: 0.3 ± 0.1 μM[11]. However, it is important to keep in mind that the value of the dissociation constant has been obtained from an association process where two exponential phases have been observed. We can further elaborate on the value of R_{eq} obtained from the fittings at the different IF7 concentrations. Since the R_{eq} is defined as the signal in the sensorgram at infinite time in the kinetic association experiment, that is, when the association equilibrium is reached, its analysis provides a strictly thermodynamic approach to determine the equilibrium K_D [44]. The fitting of the R_{eq} values (for the fastest exponential with the largest amplitude) in IF7 yielded a K_D of 0.6 ± 0.2 μM (Fig. 4 B); this value is similar, within the error, to that from fluorescence measurements (0.3 ± 0.1 μM), supporting our analysis with the fastest of the two exponentials observed.

The k_{obs}s from the second exponential yielded a linear plot with an un-acceptable $k_{off} < 0$, and a slope (k_{on}) of (0.16 ± 0.06) x 10^4 M^{-1} s^{-1}, which is almost null. At this stage, we do not know the meaning of this second kinetic process, but its small concentration-dependence suggests a uni-molecular process.

(b) *Experiments in aqueous solution at high ionic strength*: In the presence of 450 mM of NaCl, the kinetic behaviour during the association step was similar to that observed at low ionic strength (150 mM NaCl). Data were best fitted to two exponential curves, except for the highest IF7 concentrations explored (3, 5 and 10 μM) where a downwards slope was observed. However, for the lowest concentration explored (0.1 μM IF7) the curve of the association step had reached equilibrium. The pseudo-first-order plot of the fastest k_{obs} (Supplementary Material Fig. 8 A) yielded a k_{on} smaller than that measured at 150 mM NaCl and a k_{off} two-and-a-half-times larger than that at 150 mM NaCl (Table 1); these values result in a K_D of 3 ± 1 μM, which is much larger than that measured in the absence of NaCl. Thus, it seems that the affinity was reduced at high ionic strength, mainly due to a larger increase of the k_{off}, and then, we can conclude that the binding reaction is ionic-strength dependent. However, it is important to pinpoint that the R_{eq} values obtained from the fittings to the first exponential did not follow a binding curve (data not shown), suggesting that: (i) even the use of two exponentials in the association step could not take into account the full complexity of the binding reaction in the presence of high concentrations of NaCl; and (ii) at high ionic strengths, the kinetic pathway of the binding reaction seems to be modified.

(c) *Experiments in the presence of 5% TFE at 150 mM NaCl*: Many studies show an increase in affinity upon rising residual structure[45] (and references therein). As IF7 showed a 1.5-fold increase (in absolute value) in the ellipticty at 222 nm when the concentration of TFE was 5% (v/v) (Supplementary Material Fig. 1 B inset), we decided to carry out kinetic studies under these conditions (furthermore, at this TFE concentration, the fluorescence spectrum of GS was not altered, data not shown). As it happened with the other solution conditions explored in IF7, the sensorgrams were best fitted to two-exponentials, except for the concentrations of 3 and 5 μM of IF7, where we used a single exponential and a linear term. Under these conditions the association step for the lowest IF7 concentration (0.1 μM) had reached the equilibrium. The dependence of the fastest k_{obs} upon IF7 concentrations followed a straight line (Supplementary Material Fig. 8 B). From the

pseudo-first-order plot (Table 1), the values were similar to those obtained at low NaCl concentration (see above). The value of K_D was 0.5 ± 0.1 μM, identical within the error to that determined in the absence of the co-solvent (see above). However, conversely to what happens in aqueous solution, the R_{eq} values obtained from the fittings to the first exponential did not follow a binding curve (data not shown), suggesting that even the use of two exponentials in the association step could not take into account the full complexity of the binding reaction in the presence of small amounts of TFE. We do not know if this is due to the fact that TFE increased the helicity in other regions not involved in binding to GS, or alternatively because the helical population, under these conditions, is not high enough even in the IF7 regions involved in binding to GS.

The kinetic parameters of the binding reaction of IF17 to GS

Although the presence of IF7 is enough to inactivate GS *in vitro*, the presence of IF17 together with IF7, reinforces GS inactivation *in vivo*[5]. We wondered whether the binding reaction of IF17 to GS had similar association and/or dissociation rates to those of IF7. However, it is important to bear in mind that the measurements of IF17 were carried in the presence of 0.3 M urea (which affects solution viscosity[46]) (Fig. 5 A). The association steps for the sensorgrams were fitted to two exponentials at all the explored IF17 concentrations. Therefore, the binding does not follow a 1:1 kinetic two-state model: $\underset{(free)}{GS} + IF17 \underset{k_{off}}{\overset{k_{on}[IF17]}{\rightleftharpoons}} \underset{(complex)}{GS:IF17}$. The linear dependence of the fastest k_{obs} upon IF17 concentrations was worse than for IF7 (Fig. 5 B), especially at the higher protein concentrations. We obtained a k_{on} of (1.4 ± 0.5) x 10^4 M^{-1} s^{-1} (smaller than that of IF7 at 150 mM NaCl) and a k_{off} of (2.1 ± 0.8) x 10^{-2} s^{-1} (similar to that of IF7) (Table 1). These results yield a K_D of 1.5 ± 0.5 μM, similar to the value of 1 μM from equilibrium fluorescence titrations[12]. Due to the presence of urea in the solution, we tried to fit the k_{obs} to a model which takes into account mass transport effects[47], but the goodness of the fitting was similar to that of the simplest pseudo-first order conditions. Finally, it is important to note that the values of R_{eq} obtained from the fastest

association-step did not follow a binding curve (data not shown), suggesting that even the use of two exponentials could not take into account the full complexity of the IF17-GS binding reaction.

DISCUSSION

Kinetic features of the binding of IFs to GS

It has been argued that some IDPs should have a low affinity with a high specificity and then association rate constants, k_{on}, very large, close to the diffusion-limited reaction[18,45,48,49]. The k_{on} for a diffusion-limited reaction between two proteins can be predicted with a simple model[19,50]. Such approach considers the proteins as two uniformly reactive species, which diffuse freely in solution with an upper k_{on} limit of 10^9 M^{-1} s^{-1} [51]. However, proteins are not uniformly reactive over their entire surface and they must rotate to acquire a correct orientation to collide with the other protein. This rotational diffusion decreases the limit of k_{on} by several orders of magnitude leading to a range of 10^5-10^6 M^{-1} s^{-1} for the diffusion-limited reactions[52]. This value is still larger than the k_{on} measured for the binding between IF7 and GS (47000 M^{-1} s^{-1}), indicating that the reaction between both proteins is not diffusion-limited, under our conditions.

The value of the k_{on} of IF7 for the fastest process is, however, within the same order of magnitude than those of other proteins, where one of the partners is also an IDP of similar size to IF7 (i.e., less than 100-residues), and measured by biosensor-using technology[53-55]. This IF7 k_{on} is three-times larger than that of IF17 (47000 *versus* 14000 M^{-1} s^{-1}), indicating that, although *in vivo*, the binding of both proteins results in a more efficient inactivation of GS, IF7 is faster than the IF17 to reach its target (and with a slightly larger affinity[11,12]). Several factors affect the values of k_{on}s: (i) diffusion (smaller in a larger polypeptide chain); (ii) conformational changes in the interacting proteins (in the two IDPs here); and, (iii) electrostatic forces (between IFs and GS). Since both IFs are disordered and the sequence of IF17 at its C-terminus is similar to that of IF7[12] (Supplementary Material Fig. 4) the differences in the apparent k_{on}s of both proteins could be due to their chain lengths and the presence of urea in IF17.

Based on the thermodynamic measurements, we have previously suggested that upon binding to GS, IF17 (and probably IF7) becomes folded[12]. It has been proposed that due to the conformational changes that occur in IDPs upon binding to their targets, there is a strong relationship between k_{on} and K_D, measured by thermodynamic means[56]. In the two IFs, we observed such relationship occurring with the plot of bone morphogenesis protein (Fig. 1B in the paper of Prakash[56]). Furthermore, we can use this plot to predict the real k_{on}s for both proteins, assuming that the values of the K_Ds thermodynamically measured are correct[11,12]. From that plot, we obtain 17000 and 5600 M^{-1} s^{-1} for IF7 and IF17, respectively, which are smaller than the apparent values obtained from BLI (47000 *versus* 14000 M^{-1} s^{-1}). Thus, the folding of both IFs upon binding to GS slows down their association rates.

The value of k_{on} in IF7 showed a strong dependence on the concentration of NaCl: it decreased three-times as the concentration of NaCl was increased two-fold, indicating that the binding is governed by electrostatic interactions. Concomitantly, the k_{off} increased two-and-a-half-times at high NaCl, which was mainly responsible for the larger increase of K_D in 450 mM NaCl. This electrostatic dependence has been observed in other protein-protein interactions, involving either IDPs or fully ordered proteins[15,16,52,57]. However, at this stage, we cannot rule out that the presence of 450 mM NaCl could induce a compaction of the IF7 polypeptide chain or even a shift in the population of the conformers, as it has been described in other IDPs and polymers at high ionic strength[58-61].

Unfortunately, kinetic mechanisms cannot be proved, instead they can be only ruled out. Based on the fact that we had to use two exponentials in the fitting of the association step for both proteins, we suggest that both IFs do not follow a two-state model of binding to GS. In other words, the kinetic mechanism is not: $\underset{(free)}{GS} + IF \underset{k_{off}}{\overset{k_{on}[IF]}{\rightleftharpoons}} \underset{(complex)}{GS:IF}$; in fact, other IDPs show complex kinetics, with the presence of several exponential phases during association steps[33,62-64]. Instead, the binding

of both IFs to GS might entail: (i) the formation of an intermediate (the complex species marked with the asterisk below), where the folding of the IF is completed after binding to GS ($\underset{(free)}{GS + IF} \underset{k_{off}}{\overset{k_{on}[IF]}{\rightleftarrows}} GS:IF* \underset{k_{off}*}{\overset{k_{on}*}{\rightleftarrows}} \underset{(complex)}{GS:IF}$); or (ii) the pre-selection of a populated partially folded conformation in the IF pool (IF_{folded}) which is capable of binding to GS: $\underset{(unfolded)}{IF} \underset{k_{off}'}{\overset{k_{on}'}{\rightleftarrows}} \underset{(folded)}{IF} \underset{k_{off}}{\overset{k_{on}[IF_{folded}]}{\rightleftarrows}} \underset{(complex)}{GS:IF}$. At this stage, we do not know which of the two binding mechanisms is followed by both IFs. The finding that we are observing (at low NaCl concentration for the IF7-GS reaction) a second kinetic phase (with a smaller amplitude) which is almost IF7-concentration-independent (Supplementary Material Fig 7 B) could be either due to the second step in the first mechanism $GS:IF* \underset{k_{-a}*}{\overset{k_a*}{\rightleftarrows}} \underset{(complex)}{GS:IF}$, or alternatively to the first step in the second mechanism: $\underset{(unfolded)}{IF} \underset{k_{-a}'}{\overset{k_a'}{\rightleftarrows}} \underset{(folded)}{IF}$.

The above mechanisms are called folding-after-binding (or induced-fit)[63], and conformational selection (which is identical to Monod-Wyman-Changeaux model[65]), respectively. In practice, a combination of both mechanisms is also possible[66], which can be further altered by the concentration of binding (ligand) protein[63,67]. We are tempted to suggest that, given the high helical SSP of IF7 at its N terminus, the conformational selection mechanism could be prevalent in binding of both IFs to GS[68] (because of the sequence similarity (Supplementary Material Fig. 4)). This hypothesis is consistent with helical structure formation, which occurs on a μs time scale[69], much faster than the association time constant for IF7 (2.1 s = 1/(47600 M^{-1} s^{-1} x 10 x 10^{-6} M). However, the existence of such low-populated, folded conformations in IDPs does not imply that folding-upon-binding occurs through the conformational selection mechanism, as it has been shown in some IDPs[49,70]. In fact, the

mechanism of binding of both IFs to GS, due to their different lengths, non-conserved residues and the additional ones at the N terminus of IF17[12], could be fully different between both species [71].

Structure-activity relationships in binding of GS to IF7

We have mentioned that due to the strong dependence of the association kinetics rate with NaCl concentration, ionic interactions intervene in the binding of GS to IF7. We have observed that the residues of IF7 that are firstly involved in the binding to GS were Gln6 and Ser27. These residues can form hydrogen-bonds with their side-chains involving other biomolecules. However, upon a larger addition of GS, Gln4, Gln5, Ala7, Arg8, Met12, Gln16, Gln46, Phe53, Arg59 and Ser63 were also involved in binding. These results suggest that: (i) even in equilibrium conditions (as those reported by NMR) the binding is not two-state, since different residues bind differently, supporting our kinetic data; and, (ii) binding involves both electrostatic and hydrophobic contacts, also observed in other large protein-protein complexes[72]. The fact that different residues bind at different stages to GS suggests the presence of a partially-bound IF7 species, and thus an intermediate during the binding. Then our findings might indicate the presence of a GS:IF* complex (see above).

Mutational studies of IF7 have shown that substitution of Arg8, Arg21 and Arg28 by glutamic acid abolishes the ability of the mutant protein to inactivate GS[73]. In addition, molecular modelling of the binding of IF7 to GS with a short fragment of IF7, comprising its first 38 residues, suggests that residues Arg8, Arg21 and Arg28 are involved in binding to GS[74]; it is interesting to note that two of them belong to the polypeptide region that has been predicted to acquire helical secondary structure (Fig. 2, middle and bottom panels). We could only observe Arg8 at pH 7.0, since the other two residues are highly solvent-exposed (Fig. 3), and thus, our NMR experiments support the importance of Arg8 in the binding to GS.

We suggest that the formation of GS-IF complexes is characterized by a minimal interface, which from the mutational studies would involve highly charged residues. This minimal interface would serve as an anchor point for the complex formation. This intermediate complex (with a partially bound IF7) would be fixed at a later step by hydrophobic contacts, as proposed to occur in otherwise complexes of IDPs[75]. Under this hypothesis, the surface of GS would not provide a simple set of constraints that would force the folding of IFs, but rather the surface of GS would act as a facilitator of folding[76]. The facilitation and the environment provided by the hexameric rings of GS seem to be critical for both IFs, since IF7 is not capable of acquiring a well-fixed helix-like structure (low populated when the protein is isolated in solution) even in the presence of the hydrophobic environment granted by TFE.

ACKNOWLEDGEMENTS

We thank the four anonymous reviewers for helpful suggestions and discussions. We deeply thank May García, María del Carmen Fuster and Javier Casanova for technical assistance.

SUPPORTING INFORMATION AVAILABLE

Figures containing the fluorescence and CD TFE titration of IF7 at pH 4.5 (Fig. 1); the structural features of IF7 in the presence of 60% TFE (Fig. 2); the ^{1}H-^{15}N HSQC and CON of IF17 (Fig. 3); the sequence alignment of IF7 and IF17 by using Blast and Clustal (Fig. 4); the temperature study of IF7 at two different pHs (Fig. 5); the pH-titrations of GS as monitored by fluorescence and CD (Fig. 6); the sensorgrams and the pseudo-first-order plots for binding of IF7 to GS in aqueous solution at low ionic strength (Fig. 7); and the pseudo-first order plots for binding of IF7 to GS in 450 mM NaCl and in 5% TFE, 150 mM NaCl (Fig. 8). The figures are available free of charge at http:// www.acs.pub.org.

REFERENCES

1. Leigh, J. A., and Dodsworth, J. A. (2007) Nitrogen regulation in bacteria and archaea. *Annu. Rev. Microbiol. 61*, 349-377.

2. Luque, I., and Forchammer, K. A. (2008) Nitrogen assimilation and C/N balance sensing, in *The cyanobacteria: molecular biology, genetics and evolution* (Herrero, A. and Flores, E., Eds.), pp. 335-382. Caister Academic Press, Norwich, UK.

3. Muro-Pastor, M. I., Reyes, J. C., and Florencio, F. J. (2005) Ammonium assimilation in cyanobacteria. *Photosynt. Res. 83*, 135-150.

4. Reitzer, L. (2003) Nitrogen assimilation and global regulation in *Escherichia coli*. *Annu. Rev. Micobiol. 57*, 155-176.

5. García-Domínguez, M., Reyes, J. C., and Florencio, F. J. (1999) Glutamine synthetase inactivation by protein-protein interaction. *Proc. Natl. Acad. Sci. USA 96*, 7161-7166.

6. Reyes, J. C., and Florencio, F. J. (1995) A novel mechanism of glutamine synthetase inactivation by ammonium in the cyanobacterium *Synechocystis* sp. PCC 6803: involvement of an inactivating protein. *FEBS Lett. 367*, 45-48.

7. Galmozzi, C. V., Saelices, L., Florencio, F. J., and Muro-Pastor, M. I. (2010) Posttranscriptional regulation of glutamine synthetase in the filamentous cyanobacterium *Anabaena* sp. PCC 7120: differential expression between vegetative cells and heterocysts. *J. Bacteriol. 192*, 4701-4711.

8. Galmozzi, C. V., Fernández-Avila, M. J., Reyes, J. C., Florencio, F. J., and Muro-Pastor, M. I. (2007) The ammonium-inactivated cyanobacterial glutamine synthetase I is reactivated *in vivo* by a mechanism involving proteolytic removal of its inactivating factors. *Mol. Microbiol. 65*, 166-179.

9. García-Domínguez, M., Reyes, J. C., and Florencio, F. J. (2000) NtcA represses transcription of gifA and gifB genes that encode inhibitors of glutamine synthetase type I from *Synechocystis* sp. PCC 6803. *Mol. Microbiol. 35*, 1192-1201.

10. Herrero, A., Muro-Pastor, A.M., and Flores, E. (2001) Nitrogen control in cyanobacteria. *J. Bacteriol. 183*, 41-425.

11. Muro-Pastor, M. I., Barrera, F. N., Reyes, J. C., Florencio, F. J., and Neira, J. L. (2003) The inactivating factor of glutamine synthetase IF7 is a natively unfolded protein. *Protein Sci. 12*, 1443-1454.

12. Saelices, L., Galmozzi, C. V., Florencio, F. J., Muro-Pastor, M. I., and Neira, J. L. (2011) The inactivating factor of glutamine synthetase IF17 is an intrinsically disordered protein, which folds upon binding to its target. *Biochemistry 50*, 9767-9778.

13. Wright, P. E., and Dyson, H. J. (2015) Intrinsically disordered proteins in cellular signalling and regulation. *Nat. Rev. Mol. Cell Biol. 16*, 18-29.

14. Zhou, H. X. (2011) Intrinsic disorder: signalling via highly specific but short-lived association. *Trends Biochem. Sci. 37*, 43-48.

15. Rogers, J. M., Steward, A., and Clarke, J. (2013) Folding and binding of an intrinsically disordered protein: fast but not "diffusion-limited". *J. Am. Chem. Soc. 135*, 1415-1422.

16. Shammas, S. L., Travis, A. J., and Clarke, J. (2103) Remarkably fast coupled folding and binding of the intrinsically disordered transactivation domain of ccMyb to CBP KIX. *J. Phys. Chem. 117*, 13346-13356.

17. Shammas, S. L., Rogers, J. M., Hill, S. A., and Clarke, J. (2012) Slow, reversible, coupled folding and binding of the spectrin tetramerization domain. *Biophys. J. 103*, 2203-2214.

18. Dogan, J., Jonasson, J., Andersson, E., and Jemth, P. (2015) Binding rate constants reveal distinct features of disordered protein domains. *Biochemistry 54*, 4714-4750.

19. Berg, O. G., and von Hippel, P. H. (1985) Diffusion controlled macromolecular interactions. *Annu. Rev. Biophys. Biophys. Chem. 14*, 131-160.

20. Gill, S.C., and von Hippel, P.H. (1989) Calculation of protein extinction coefficients from amino acid sequence data. *Anal. Biochem. 182*, 319-326.

21. Cavanagh, J., Fairbrother, W.J., Palmer, A.G. 3rd, and Skelton, N. (1996) *Protein NMR spectroscopy. Principles and Practice* (1st ed), Academic Press, NY.

22. Pantoja-Uceda, D., and Santoro, J. (2013) Direct correlation of consecutive C'-N groups in proteins: a method for the assignment of intrinsically disordered proteins. *J. Biomol. NMR 57*, 57-63.

23. Pantoja-Uceda, D., and Santoro, J. (2008) Amino acid type identification in NMR spectra of proteins via beta- and gamma-carbon edited experiments. *J. Magn. Reson. 195*, 187-195.

24. Pantoja-Uceda, D., and Santoro, J. (2012) New amino acid residue type identification experiments valid for protonated and deuterated proteins. *J. Biomol. NMR 54*, 145-153.

25. Delaglio, F., Grzesiek, S., Vuister, G.W., Zhu, G., Pfeifer, J., and Bax, A. (1995) NMRPipe: a multidimensional spectral processing system based on UNIX pipes. *J Biomol. NMR 6*, 277-293.

26. Johnson, B.A., and Blevins, R.A. (1994) NMR view: a computer program for the visualization and analysis of NMR data. *J. Biomol. NMR 4*, 603-614.

27. Wishart, D.S., Bigam, C.G., Yao, J., Abildgaard, F., Dyson, H.J., Oldfield, E., Markley, J. L., and Sykes, B. D. (1995) ^{1}H, ^{13}C and ^{15}N chemical shift referencing in biomolecular NMR. *J. Biomol. NMR 6*, 135-140.

28. Frenzel, D., and Willbolds, D. (2014) Kinetic titration series with biolayer interferometry. *PLoS ONE 9*, e106882.

29. Nice, E. C., and Catimel, B. (1999) Instrumental biosensors: new perspectives for the analysis of biomolecular interactions. *BioEssays 21*, 339-352.

30. Karlsson, R., Michaelsson, A., and Mattson, L. (1991) Kinetic analysis of monoclonal antibody-antigen interactions with a new biosensor based analytical system. *J. Immunol. Methods 145*, 229-240.

31. O'Shanessy, D. J., Brigham-Burke, M., Sonenson, K., Hensley, P., and Brooks, I. (1993) Determination of rate and equilibrium binding constants for macromolecular interactions using surface plasmon resonance: use of nonlinear least squares analysis methods. *Anal. Biochem. 212*, 457-468.

32. Zheng, X., Bi, C., Li, Z., Podariu, M., and Hage, D. S. (2015) Analytical methods for kinetic studies of biological interactions: a review. *J. Pharm. Biomed. Anal. 113*, 163-180.

33. O'Shannessy, D. J., and Winzor, D. J. (1996) Interpretation of deviations from pseudo-first-order kinetic behaviour in the characterization of ligand binding by biosensor technology. *Anal. Biochem. 236*, 275-283.

34. Camilloni, C. De Simone, A., Vranken, W. F., and Vendruscolo, M. (2012) Determination of secondary structure populations in disordered states of proteins using nuclear magnetic resonance chemical shifts. *Biochemistry 51*, 2224-2231.

35. Sormanni, P., Camilloni, C., Fariselli, P., and Vendruscolo, M. (2015) The s2D method: simultaneous sequence-based prediction of the statistical populations of ordered and disordered regions in proteins. *J. Mol. Biol.* 427, 982-996.

36. Khan, S. N., Charlier, C., Augustyniak, R., Salvi, N., Déjean, V., Bodenhausen, G., Lequin, O., Pelupessi, P., and Ferrange, F. (2015) Distribution of pico- and nanosecond motions in disordered proteins from nuclear spin relaxation. *Biophys. J. 109*, 968-999.

37. Buck, M. (1998) Trifluoroethanol and colleagues: co-solvents come of age. *Q. Rev. Biophys. 31*, 297-355.

38. Jackson, S. E. (1996) How do small proteins fold? *Fold Des. 3*, R81-R91.

39. Altschul, S. F., Madden, T. L., Schäffer, A. A., Zhang, J., Zhang, Z., Miller, W., and Lipman, D. J. (1997) Gapped BLAST and PSI-BLAST: a new generation of protein database search programs *Nucl. Acids. Res. 25*, 3389-3402.

40. Gouoj, M., McWiliam, H., Li, W., Valentin, F., Squizzato, S., Paern, and López, R. (2010) A new bioinformatics analysis tools framework at EMBL-EBI. *Nucl. Acids. Res. 38*, W695-W699.

41. Kjaergaard, M., Nørholm, A.-B., Hendus-Altenbuger, R., Pedersen, S. F., Poulsen, F. M., and Kragelund, B. B. (2010) Temperature-dependent structural changes in intrinsically disordered proteins: formation of α-helices or loss of polyproline II? *Protein Sci. 19*, 1555-1564.

42. Englander, S.W., and Kallenbach, N.R. (1984) Hydrogen exchange and structural dynamics of proteins and nucleic acids. *Q. Rev. Biophys. 16*, 521-655.

43. Gill, H. S., Pfluegl, G. M., and Eisenberg, D. (2002) Multicopy crystallographic refinement of a relaxed glutamine synthetase from *Mycobacterium tuberculosis* highlights flexible loops in the enzymatic mechanism and regulation. *Biochemistry 41*, 9863-9872.

44. Schuck, P., and Minton, A. P. (1996) Kinetic analysis of biosensor data: elementary tests for self-consistency. *Trends Biochem. Sci. 21*, 458-460.

45. Shammas, S. L., Crabtree, M. D., Dahal, L., Wicky, B. I. M., and Clarke, J. (2016) Insights into coupled folding and binding mechanisms from kinetic studies. *J. Biol. Chem. 291*, 6689-6695.

46. Kawahara, K., and Tanford, C. (1966) Viscosity and density of aqueous solutions of urea and guanidine hydrochloride. *J. Biol. Chem. 241*, 3228-3232.

47. Schuck, P., and Minton, A. P. (1996) Analysis of mass transport-limited binding kinetics in evanescent wave biosensors. *Anal. Biochem. 240*, 262-272.

48. Gianni, S., Dogan, J., and Jemth, P. (2016) Coupled binding and folding of intrinsically disordered proteins: what can we learn from kinetics? *Curr. Opin. Struct. Biol. 36*, 18-24.

49. Dogan, J., Gianni, S., and Jemth, P. (2014) The binding mechanisms of intrinsically disordered proteins. *Phys. Chem. Chem. Phys.16*, 6323-6331.

50. Zhou, H. X. (1993) Brownian dynamics study of the influences of electrostatic interaction and diffusion on protein-protein association kinetics. *Biophys. J. 64*, 1711-1726.

51. Atkins, P. W., and De Paula, J. (2008) *Physical chemistry for the life sciences* (1st Ed.). W. H Freeman, pp 279-280.

52. Schreiber, G., Haran, H., and Zhou, H. X. (2009) Fundamental aspects of protein-protein association kinetics. *Chem. Rev. 109*, 839-860.

53. Zanier, K., Charbonnier, S., Baltzinger, M., Nominé, Y., Altschuh, D., and Travé G. (2005) Kinetic analysis of the interactions of human papillomavirus E6 oncoproteins with the ubiquitin ligase E6AP using surface plasmon resonance. *J. Mol. Biol. 349*, 401-412.

54. Yu, X., Wang, Q. Y., Guo, Y., Dolmer, K., Young, J. A. T., Gettings, P. G. W., and Rong, L. (2003) Kinetic analysis of binding interaction between the subgroup A Rous sarcoma virus glycoprotein SU and its cognate receptor Tva: calcium is not required for ligand binding. *J. Virol. 77*, 7517-7526.

55. Catimel, B., Trazel, T., Fontes, M. R. M., Jennings, I. G., Jans, D. A., Howlett, G. J., Nice, E. C., and Kobe, B. (2001) Biophysical characterization of interactions involving importin-α during nuclein import. *J. Biol. Chem. 276*, 34189-34198.

56. Prakash, M. K. (2011) Insights on the role of (dis)order from protein-protein interaction linear free-energy relationships. *J. Am. Chem. Soc. 133*, 9976-9979.

57. Ganguly, D., Otieno, S., Waddell, B., Iconaru, L., Kriwacki R. W., and Chen, J. (2012) Electrostatically accelerated coupled binding and folding of intrinsically disordered proteins. *J. Mol. Biol. 422*, 674-684.

58. Müller-Späth, S., Soranno, A., Hirschfeld, V., Hofmann, H., Rüegger, S., Reymond, L., Nettels, D., and Schuler, B. (2010) From the cover: Charge interactions can dominate the dimensions of intrinsically disordered proteins. *Proc. Natl. Acad. Sci. USA 107*, 14609-14614.

59. Neira, J. L., Rizzuti, B., and Iovanna, J. L. (2016) Determinants of the pK_a values of ionizable residues in an intrinsically disordered protein. *Arch. Biochem. Biophys. 598*, 18-27.

60. Dobrynin, A. V., and Rubinstein, M. (2005) Theroy of polyelctrolytes in solutions and at surfaces. *Prog. Polym. Sci. 30*, 1049-1118.

61. Dobrynin, A. V., Rubinstein, M., and Obhukov, S. P. (1996) Cascade of transitions of polyelectrolytes in poor solvents. *Macromolecules 29*, 2974-2979.

62. Chemes, L. B., Sánchez, I. B., and de Prat Gay, G. (2011) Kinetic recognition of the retinoblastoma tumor suppressor by a specific protein target. *J. Mol. Biol. 412*, 267-284.

63. Kiefhaber, T., Bachmann, A., and Jensen, K. S. (2012) Dynamics and mechanisms of coupled protein folding and binding reactions. *Curr. Opin. Struct. Biol. 22*, 21-29.

64. Fisher, R. J., Fivash, M., Casas-Finet, J., Erickson, J. W., Kondoh, A., Bladen, S. V., Fisher, C., Watson, D.K., and Papas, T. (1994) Real-time DNA binding measurements of the ETSl recombinant oncoproteins reveal significant kinetic differences between the p42 and p51 isoforms. *Protein Sci. 3*, 257-266.

65. Monod, J., Wyman, J., and Changeux, J. P. (1965) On the nature of allosteric transitions: a plausible model. *J. Mol. Biol. 12*, 88-118.

66. Espinoza-Fonseca, L. M. (2009) Reconciling binding mechanisms of intrinsically disordered proteins. *Biochem. Biophys. Res. Commun. 382*, 479-482.

67. Hammes, G. G., Chang, Y. C., and Oas, T. G. (2009) Conformational selection or induced fit: a flux description of reaction mechanism. *Proc. Natl. Acad. Sci. USA 106*, 13737-13741.

68. Fuxreiter, M., Simon, I., Friedrich, P., and Tompa, P. (2004) Pre-formed structural elements feature in partner recognition by intrinsically unstructured proteins. *J. Mol. Biol. 338*, 1015-1026.

69. Davis, C. M., Cooper, A. K., and Dyer, R. B. (2015) Fast helix formation in the B domain of protein A revealed by site-specific infrared probes. *Biochemistry 54*, 1758-1766.

70. Dosnon, M., Bonettu, D., Morrone, A., di Silvio, E., Longhi, S., and Gianni, S. (2015) Demonstration of a folding after binding mechanism in the recognition between the measles virus NTAIL and X domains. *ACS Chem. Biol. 10*, 795-802.

71. Arai, M., Sugase, K., Dyson, H. J., and Wright, P. E. (2015) Conformational propensities of intrinsically disordered proteins influence the mechanism of binding and folding. *Proc. Natl. Acad. Sci. USA 112*, 9614-9619.

72. Mukrasch, M. D., Bibow, S., Korukottu, J., Jeganathan, S., Biernat, J, Griesinger, C., Mandelkow, E., and Zweckstetter, M. (2009) Structural polymorphism of 441-residue tau at single residue resolution. *PLoS Biol. 7*, e1000034.

73. Saelices, L., Galmozzi, C. V, Florencio, F. J., and Muro-Pastor, M. I. (2011) Mutational analysis of the inactivating factors IF7 and IF17 from *Synechocystis* sp. PCC 6803: critical role of arginine amino acid residues for glutamine synthetase inactivation. *Mol. Microbiol. 82*, 964-975.

74. Saelices, L., Robles-Rengel, R., Florencio, F. J., and Muro-Pastor, M. I. (2015) A core of three amino acids at the carboxyl-terminal region of glutamine synthetase defines its regulation in cyanobacteria. *Mol. Microbiol. 96*, 483-496.

75. Sharma, R., Raduly, Z., Miskei, M., and Fuxreiter, M. (2015) Fuzzy complexes: specific binding without complte unfolding. *FEBS Lett. 589*, 2533-2542.

76. Drobnak, I., De, J., Haesaerts, S., Vesnaver, G, Loris, R., and Lah, J. (2013) Energetic basis of uncoupling folding for an intrinsically disordered protein. *J. Am. Chem. Soc. 135*, 1288-1294.

Table 1: Measured k_{on}s and k_{off}s of IF7 and IF17 to biosensor-bound GS by BLI[a]

Solution conditions and proteins	k_{on} (x 10^4) (M^{-1} s^{-1})	k_{off} (x 10^{-2}) (s^{-1})
IF7 in aqueous solution (150 mM NaCl)	4.7 ± 0.2	1.9 ± 0.8
IF7 in aqueous solution (450 mM NaCl)	1.7 ± 0.3	5 ± 1
IF7 in 5% TFE (150 mM NaCl)	3.92 ± 0.06	2.2 ± 0.2
IF17 in aqueous solution (0.3 M urea and 150 mM NaCl)	1.4 ± 0.5	2.1 ± 0.8

[a]Experiments were acquired at 25 ºC. Errors are fitting errors from the fittings of the pseudo-first-order plots (Supplementary Material Figs. 7 and 8).

FIGURE LEGENDS

FIGURE 1: **^{1}H-^{15}N HSQC spectrum of IF7**. The assignment of IF7 is shown. Signals with an asterisk correspond to folded peaks. Signals with a negative number in lower case correspond to residues in the His-tag (with sequence SSGLVPRGSH). The spectrum was acquired in a Bruker AV 800, at pH 4.5 and 25 ºC.

FIGURE 2: **Relaxation and sequence analysis of IF7**. (Top) NOE ratios of IF7 at 800 MHz (grey line) and 500 MHz (black line). The dashed lines correspond to one standard deviation above the mean NOE value obtained disregarding the last two C-terminal residues. Errors are assumed to be 10% of the value of NOE. (Middle) Secondary structure propensity (SSP) obtained from δ2D software[34] using the assignment of IF7. (Bottom) SSP obtained by using s2D software[35] and the primary structure of IF7.

FIGURE 3**: Titration of IF7 with GS.** (A) ^{1}H-^{15}N TROSY spectra of isolated IF7 (130 μM) at different concentrations of GS (indicated in different colours). (B) Absolute decrease of intensities of the signals in the ^{1}H-^{15}N TROSY spectra of IF7 in the absence and in the presence of increasing amounts of GS. An asterisk indicates that the intensity could not be unambiguously determined due to overlapping. Spectra were acquired in the Bruker AV-800 at 20 ºC and pH 7.0.

FIGURE 4: **Kinetics of the binding between GS and IF7 as monitored by BLI.** (A) Sensorgrams at the different concentrations of IF7 used (pseudo-first order conditions). The first 180 seconds correspond to the first equilibration step, loading of biosensor with GS and equilibration with the buffer. (B) Plot of the steady state response, R_{eq}, *versus* the IF7 concentration for determination of the

binding affinity, K_D. The line through the data is the fitting to a binding 1:1 curve. Experiments were carried out at 25 ºC.

FIGURE 5: **Kinetics of the binding between GS and IF17 as monitored by BLI.** (A) Sensorgrams at the different concentrations of IF17 used (pseudo-first order conditions). The first 150 seconds correspond to the loading of biosensor with GS and equilibration with the buffer. (B) Dependence of the k_{obs} upon IF17 concentrations. Experiments were carried out at 25 ºC.

Fig. 1 (Pantoja-Uceda et al.)

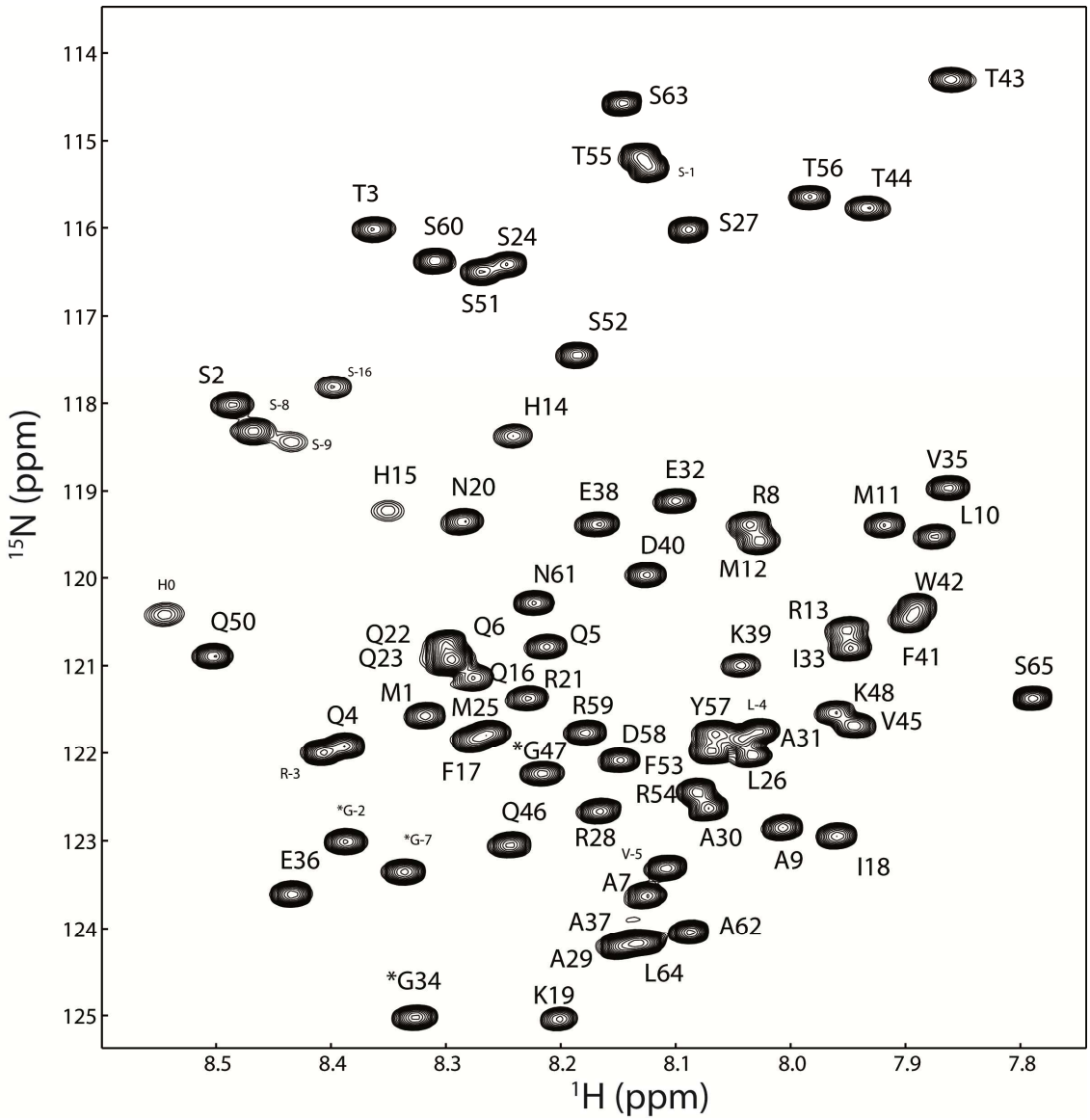

Fig. 2 (Pantoja-Uceda et al.)

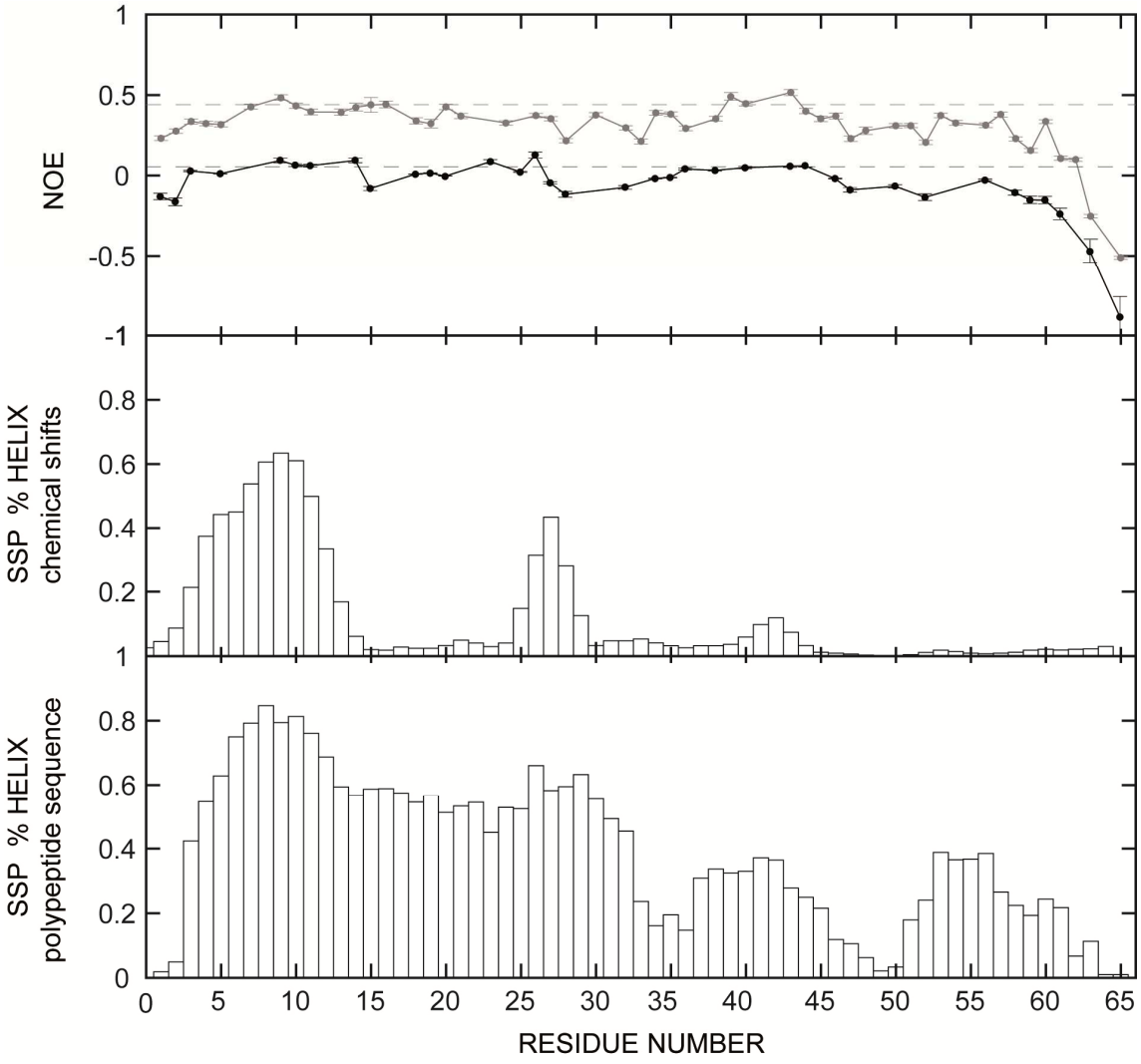

Fig. 3 (Pantoja-Uceda et al.)

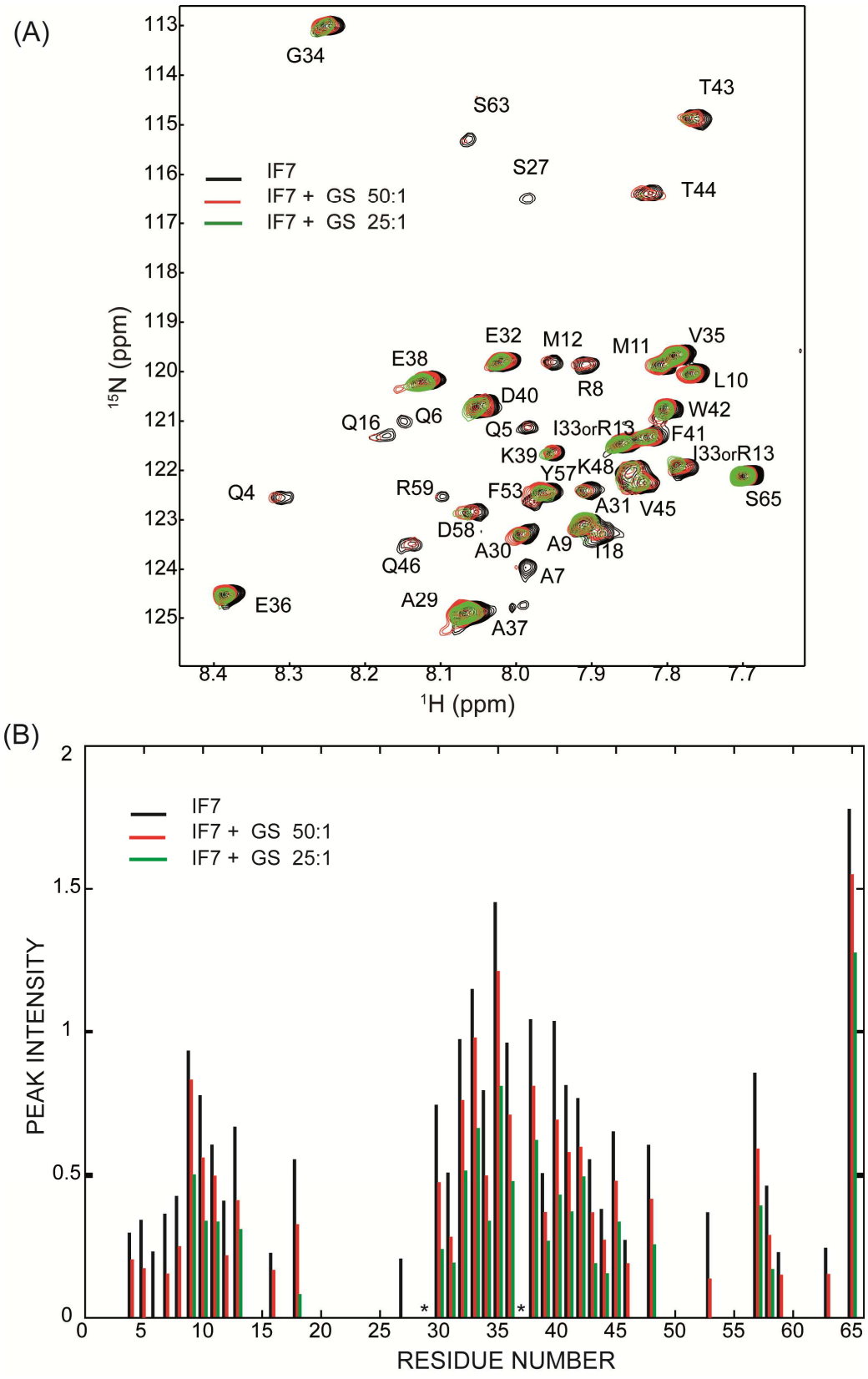

Fig. 4 (Pantoja-Uceda et al.)

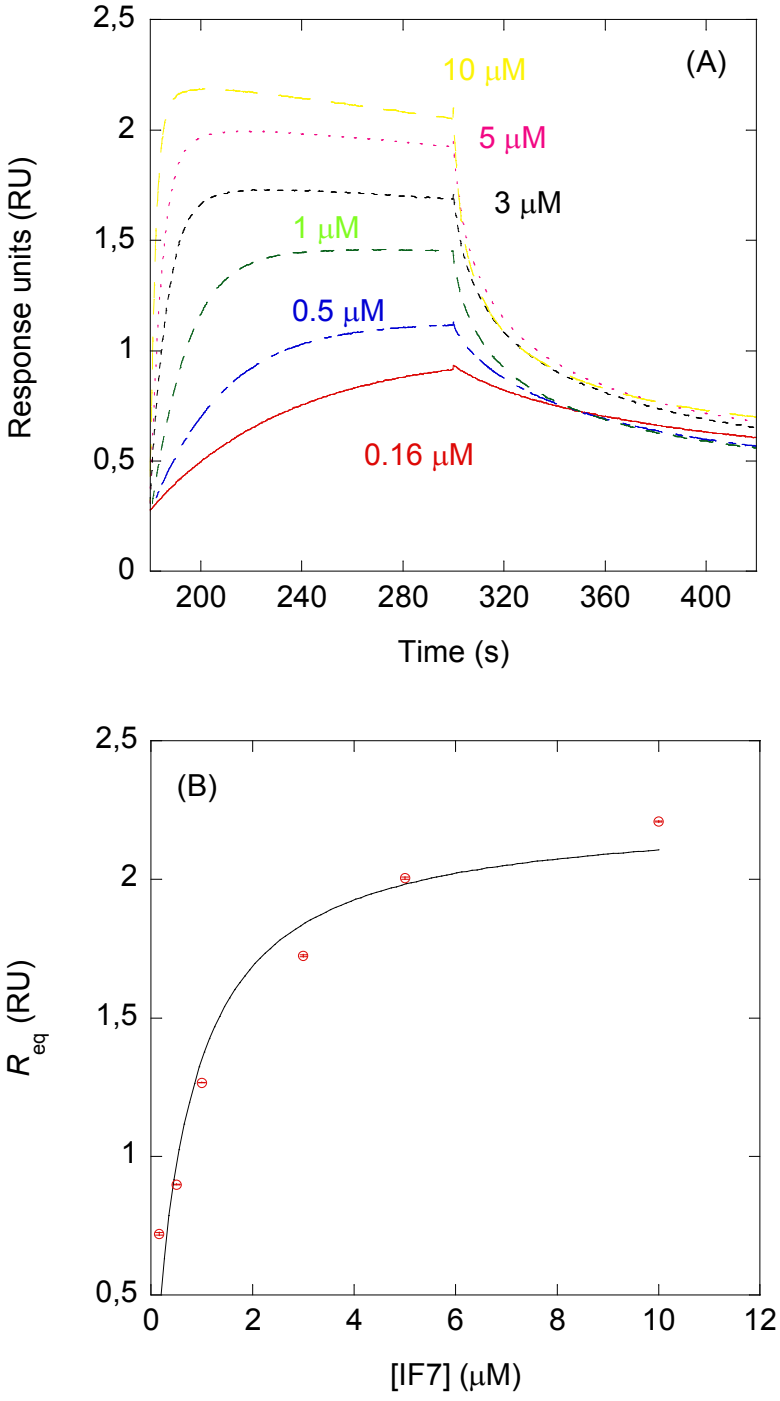

Fig. 5 (Pantoja-Uceda et al.)

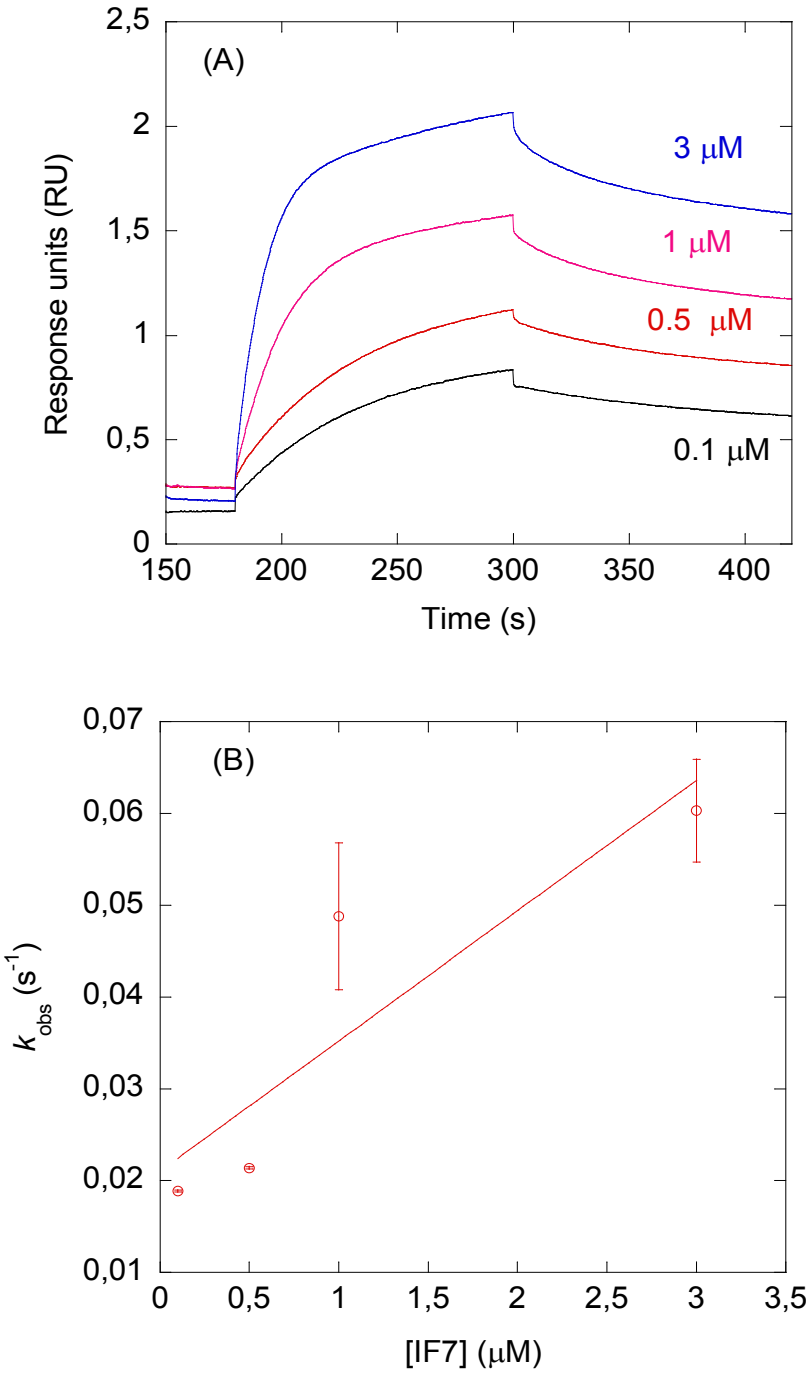

For Table of contents